Development of a radiometric sensor for the hazard assessment of scattered high-power laser radiation

Andreas Peckhaus[a], Patrick Kuhne[b], Maike Neuland[b], Thomas Hall[a], Carsten Pargmann[c] and Frank Duschek[b]

[a]German Aerospace Center (DLR), Institute of Technical Physics, Pfaffenwaldring 38-40, 70569 Stuttgart, Germany

[b]German Aerospace Center (DLR), Institute of Technical Physics, Langer Grund, 74239 Hardthausen, Germany

[c]Heilbronn University of Applied Sciences, Faculty of Mechanics and Electronics, Max-Planck-Straße 39, 74081 Heilbronn, Germany

ABSTRACT

The outdoor operation of lasers involves the potential risk of unintentionally exposing the human eye and skin to radiation. In addition to direct exposure, indirect scattered radiation of high-power lasers may pose a threat to operators, working personnel, and third parties. Hazard assessments are usually performed based on laser safety standards. However, these standards are limited in their applicability regarding outdoor environments and therefore it is advisable to corroborate models and safety calculations with measurements of the absolute scattered radiant power under realistic conditions.

For the determination of scattered radiation, a radiometric detection system has been developed. The system consists of an optical, electronic, and mechanical unit. Two realizations of the optical unit with a side-on photomultiplier tube (PMT) and a photodiode amplifier (PDA) have been built according to laser safety standards (e.g. German safety policies). Two detectors facilitate the detection of scattered radiation over a wide power range. The electronic unit contains the data acquisition and processing system and peripheral devices (i.e. environmental sensors and GPS module). A lock-in amplifier is used to reduce the contribution of unwanted background radiation. The optical and electronic units are separately housed in a weather-resistant case on a tripod and a mobile container, respectively.

Radiometric calibration is performed for each optical detection unit. The calibration involves a two-step procedure allowing for a direct conversion of the output voltage of the lock-in amplifier into an absolute scattered power considering the detector area and collection solid angle of the optical detection unit. Goniometer-based light scattering measurements of solid samples are carried out for the characterization of the performance of the optical detection system in terms of dynamic range, accuracy, reproducibility, and the influence of background noise and contribute to a better understanding of the detection system in the future field deployment.

Keywords: High-power laser, laser safety, light scattering, optical sensor

1. INTRODUCTION

By operating lasers outdoors, the question of laser safety arises due to potentially unintentional exposure to laser radiation. Not only intrabeam viewing poses a threat to the human eye, scattering and reflection of laser radiation must also be considered. In the case of the use of high-power lasers, scattered laser radiation can originate from solid/liquid surfaces or even from atmospheric constituents[1] (e.g. aerosols, precipitation). Laser safety regulations such as ANSI Z136.6 address the issue of outdoor laser operation and provide guidance for the safe use of lasers in outdoor environments.[2] However, hazard assessments purely based on laser safety standards can not capture the complexity of high-power laser applications in the field. Therefore, measurements of scattered laser radiation under environmental conditions are needed to corroborate models and safety calculations.

Correspondence to: A. Peckhaus (E-mail: andreas.peckhaus@dlr.de)

Several measuring instruments for the hazard assessment of laser radiation are described in the literature. Royston et al. presented an instrument to determine levels of accessible laser radiation and exposure duration in the visible range for continuous wave (CW) and pulsed radiation.[3] Corder et al. described an instrument with different measuring heads for different wavelengths, which can be used for CW and pulsed radiation.[4–6] The automated processing and analysis of the laser radiation allow assessing whether the maximum permissible exposure (MPE) limit has been exceeded or not. There are also commercial spectroradiometers for the hazard assessment of laser radiation for the wavelength range from 300 to 1050 nm available.[7] The difficulty of the design of a radiometric detection system is that the laser wavelength, the exposure duration, the radiant power, and the spatial distribution of the light source must be taken into account in order to assess the hazard of the radiation. Due to the large range of parameters, it is at least challenging if not impossible to develop a single detection system for all possible conditions and scenarios.[8]

Previous investigations have performed hazard analyses of scattered radiation of high-power lasers in the range of a few meters in relation to the target.[9,10] It was concluded that the intensity of scattered radiation at short distances can not be directly used to estimate the intensity at larger distances.[10] In the present study, a wavelength-specific radiometric detection system is presented, which is capable of measuring the scattered radiation from atmospheric constituents as well from an irradiated target at specified distances in outdoor environments.

The study is organized as follows: First, the design of the detection system with its components such as the optical, electronic, and mechanical units is described. Then the calibration of the detection system using an integrating sphere and a laser at 1030 nm is presented. Finally, the detection system is characterized by using solid samples with different reflection properties. The study concludes with a brief summary of the findings and an outlook.

2. DESCRIPTION OF THE DETECTION SYSTEM

The detection system is designed to fulfill specific requirements according to laser safety standards[11,12] and potential use case scenarios in outdoor locations.[1] For outdoor laser operations, the detection system should be compact, robust, and mobile and the geographic position of the system should be known accurately. It is required that the detectors have a wide dynamic range to receive scattered laser radiation from atmospheric particles and solid/liquid targets. The optical unit of the detection system should be designed in such a way that scattered laser radiation from a precisely limited field-of-view (FOV) is received by the detectors. To address these system requirements, the different parts of the detection system are described in the following.

The design of the optical unit is based on the considerations about directional radiometers by Michael Mishchenko.[13,14] By taking these considerations into account, a 280 mm long black-anodized aluminum tube was constructed, which has a 7 mm diameter aperture on each side and can be directly attached to a photodetector (see Figure 1a). A commercial 30 mm cage system with mounted optical elements can be inserted into the tube that protects the cage system against light contamination from the surrounding and reduces stray light in the interior. The scattered radiation crosses from the entrance to the exit of the optical unit an antireflection (AR)-coated biconvex lens (OSE-SLB-15B-70PIR2, Laser 2000) with 70.5 mm focal length, an adjustable iris diaphragm (CP20S, Thorlabs), a second AR-coated biconvex lens (OSE-SLB-25.4B-70PIR2, Laser 2000) acting as a relay lens, and a filter system. The filter system consists of a longpass (LP) filter (BLP01-980R-25, Semrock) and a bandpass (BP) filter (FLH1030-10, Thorlabs) at 1030 nm and can be easily exchanged via a removable cage segment depending on the application. The FOV is determined by the focal length of the first lens and the diameter of the iris diaphragm, which can be adjusted from 0.8 to 20.0 mm resulting in acceptance angles from 11 mrad to 284 mrad (see Figure 1b). An acceptance angle of 100 mrad (i.e. 5.73°)) is of particular interest as it represents the maximum limit of extended light sources considered in the hazard analysis of present laser safety standards.[11,12] It should be emphasized that the requirements of the laser safety standards (i.e. a 7 mm diameter aperture and an acceptance angle of 100 mrad) are met by the optical system.

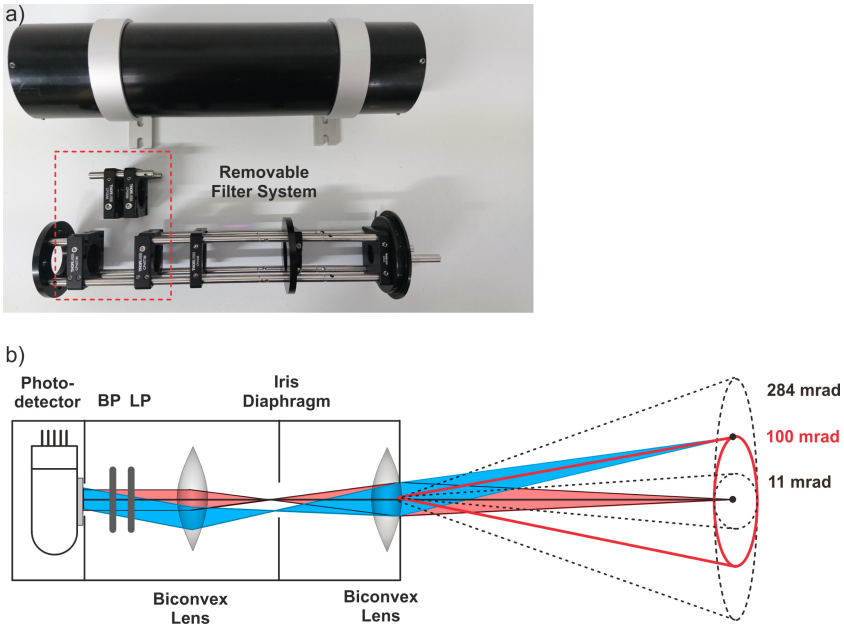

Figure 1: a) Photograph of the black-anodized aluminum tube with a removable cage segment system. b) Schematic representation of the optical unit of the detection system. The acceptance angle of 100 mrad corresponding to a solid angle of $3.13 \cdot 10^{-2} sr$ is highlighted in red.

To detect scattered laser radiation a photomultiplier tube (PMT) and a photodiode with an integrated transimpedance amplifier (TIA) are used (see Figures 2a and b). Both of the detectors are suitable to receive near-infrared radiation at 1030 nm (see Table 1), which is the central wavelength of the laser source. The PMT (R5108, Hamamatsu) is primarily chosen for aerosol scattering measurements due to its high sensitivity, whereas the photodiode amplifier (PDA100A2, Thorlabs) is used for target scattering measurements. The sensitive areas of the detectors are comparatively large to receive the total scattered radiation that falls through the 7 mm diameter aperture at the end of the tube. The detectors are light-tight connected to the tube.

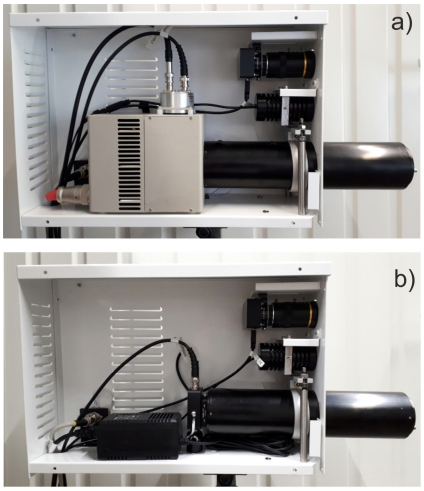

Figure 2: Photographs of the detection system with a) PMT or b) PDA installed.

Table 1: Specifications of the detectors[a]

	#1	#2
Manufacturer	Hamamatsu	Thorlabs
Model	PMT R5108	PDA100A2
Spectral range	400-1200 nm	320-1100 nm
Active Area	16 mm x 18 mm	⌀ 9.8 mm
Gain[b]	$3.0 \cdot 10^5$	0-70 dB (1-3162)
QE[c]	0.04% at 1060 nm	72.59% at 1030 nm

[a]The values are taken from datasheets of the manufacturers.
[b]The TIA of the PDA100A2 has 8 gain steps.
[c]QE denotes the quantum efficiency of the detector.

The detected signal is transmitted to a lock-in amplifier (LIA-MVD-200-L, Femto) together with the reference signal from an optical modulator (Chopper controller: MC2000B, Blade: MC1F10, Thorlabs). The lock-in amplifier acts as a narrow bandpass filter and allows to significantly suppress the contribution of the background. The voltage signal is read out by a signal-board computer (Red Pitaya STEM Lab 125-14) and transferred to the PC (ESPRIMO G558, Fujitsu). In addition, a microcontroller (Arduino Mega 2560 Rev3) is used to obtain data from different types of peripheral sensors. These sensors include two GPS modules (C94-M8P-3, U-Blox) with Real-Time Kinematic (RTK) capability, a Particulate Matter (PM) sensor (SPS30, Sensirion), and a weather sensor (BME280, Seeed Studio). A laser module (RLDD532-50-3, Roithner Lasertechnik) at 532 nm can also be controlled via a digital output port of the microcontroller to align the FOV of the detection system. Furthermore, visual information of the environment can be fed into the PC via a video camera (Raspberry Pi HQ Camera) equipped with two objectives (8-50 mm zoom lens and 6 mm wide-angle lens). The connection of the individual electronic devices of the detection system is shown in Figure 3.

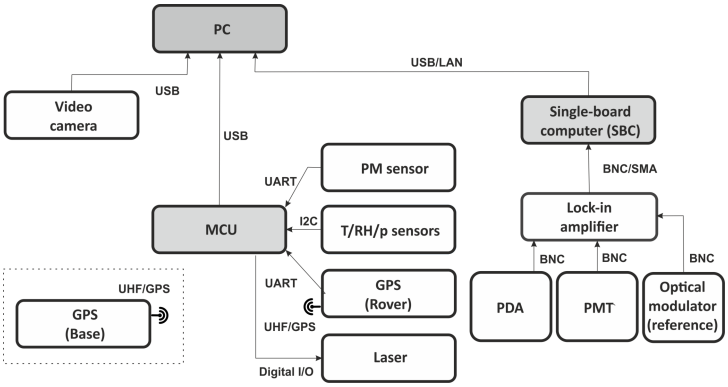

Figure 3: Schematic representation of the wiring of the electronic devices of the detection system including the specification of the interfaces.

The optical unit, the laser module, and the video camera are embedded in a self-built weatherproof housing on a tripod (see Figures 4a and b). With a gimbal head (GH2, Benro), the detection system can be vertically adjusted, inclined, and rotated around the axis of the tripod (BST-K-M, 69 - 170 cm, Stabila). On the other hand, the electronic devices are housed in a mobile case (V3515, Bawer), which is connected via a 2.5 m long cable with the optical unit (see Figure 4c). The detection system is supplied externally with power and the measurement data can be exchanged by means of remote access.

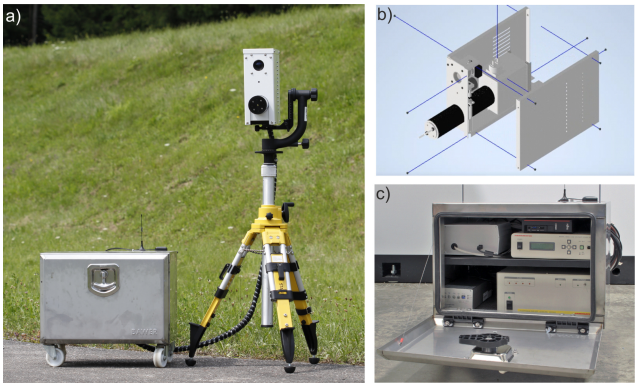

Figure 4: a) Photograph of the detection system located at the DLR laser test range in Lampoldshausen.
b) CAD drawing of the environmental housing. c) Photograph of the mobile case with the electronic devices.

3. CALIBRATION

A two-step process is used for the absolute radiometric calibration of the detection system:[15] In the first step, a free-space linearly-polarized DPSS laser at 1030 nm (1030L-11B, Integrated Optics) is attenuated with various neutral density (ND) filters and coupled into an integrating sphere (CSTM-US-100-SL, SphereOptics). The incident laser radiation is homogenized inside the integrating sphere due to multiple reflections so that its directionality is lost. In front of the exit port of the integrating sphere, a NIST-traceable calibrated spectroradiometer (PSR+3500, SpectralEvolution) is positioned, which is used to record the spectral radiance of the emitted radiation. In parallel, a cooled Si photodiode attached to the integrating sphere monitors the photocurrent. The spectral radiance of the radiation is recorded for different attenuations of the laser and different exit port diameters (i.e. 38 mm, 25 mm, and 22 mm). An exemplary measurement of the spectral radiance as a function of wavelength is shown in Figure 5a. When the spectral radiance is integrated over the wavelength range from 1000 to 1100 nm (see dashed lines in Figure 5a), then the integrated radiance can be obtained, which can be correlated to the photocurrent (see Figure 5b). Figure 5b shows a linear dependence of the integrated radiance and the photocurrent. The following proportionality factors between integrated radiance and photocurrent are determined: 345986 W/A m^2 sr (22 mm), 347559 W/A m^2 sr (25 mm) and 345485 W/A m^2 sr (38 mm). A random measurement uncertainty of 11 % is estimated.

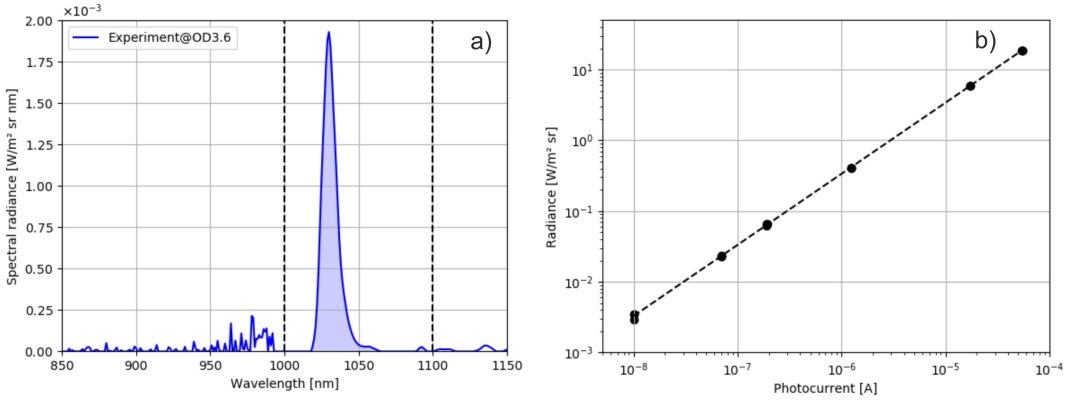

Figure 5: a) Spectral radiance of emitted radiation at the exit port of the integrating sphere as a function of wavelength. b) Integrated radiance of differently attenuated radiation as a function of the photocurrent.

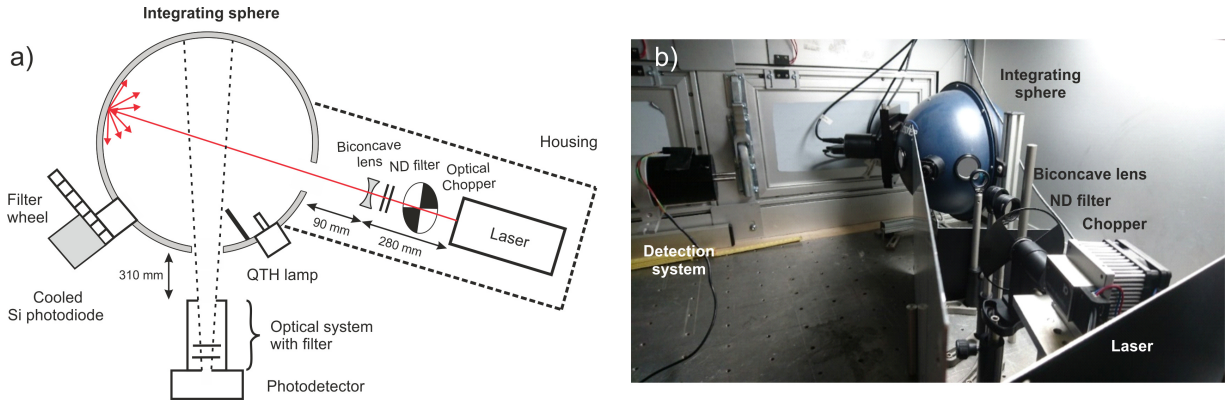

Figure 6: a) Schematic representation of the calibration setup. b) Photograph of the calibration setup in the laser safety enclosure.

In the second calibration step, a correlation is established between the photocurrent and the voltage signal of the lock-in amplifier. The DPSS laser at 1030 nm is amplitude modulated by an optical chopper with 20 Hz and attenuated with various ND filters and then fed into the integrating sphere. Before entering, the laser beam is widened by a biconcave lens to obtain a larger spot size at the inner surface of the integrating sphere. The detection system to be calibrated and the cooled Si photodiode are located at the output ports of the integrating sphere (see Figure 6). A voltage signal is recorded by the lock-in amplifier for various gain settings of the lock-in amplifier or transimpedance amplifier and various attenuations of the laser. The photocurrent of the Si photodiode is read out by a Picoammeter (6485/E, Keithley). Figure 7 shows the calibration of the detection system with the PMT and the PDA for various gain settings. With the aid of the second calibration step, calibration factors can be derived to convert the measured voltage into a current and by making recourse to the proportionality factors of the first calibration step, an absolute scattered power can be calculated under the assumption that the receiving area and the solid angle of the detection system are known.

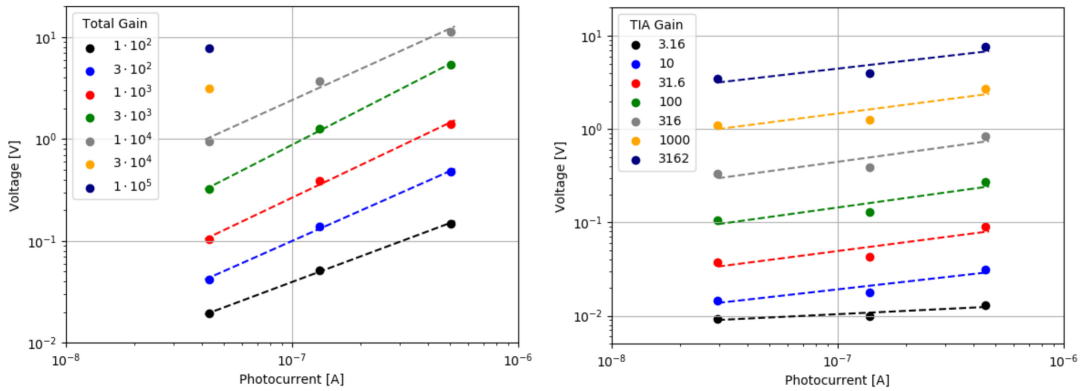

Figure 7: The voltage signal of the lock-in amplifier as a function of the photocurrent of the cooled Si photodiode for a) PMT and b) PDA. The dashed lines are linear regressions to the data.

4. CHARACTERIZATION OF THE DETECTION SYSTEM

4.1 Experimental setup

For the characterization of the detection system, a goniometer-based scatterometer has been developed to examine the angle-resolved scattering of solid samples. The setup is comparable to scatterometers described in the literature.[16] It consists of a DPSS laser at 1030 nm that is modulated with 20 Hz and attenuated before the laser beam hits the reflection targets. The incident laser power is measured with a power meter (Thermal sensor: S401C, Console: PM100D, Thorlabs) and checked before and after each measurement. The reflection targets are clamped in a sample holder, which is mounted on top of the rotation stage. The rotation stage can be rotated by 360°. The sample holder can be independently rotated and is set to a fixed angle of incidence of $\theta_i = 30°$ for the light scattering measurements. The scattering measurements are performed in the scattering plane, i.e. there is no azimuthal dependence ($\phi_s = 0°$ and $\phi_i = 180°$). The scattered radiation is recorded by the detection system, which is positioned at a distance of 20 cm from the target (see Figure 8). For the light scattering measurements, the voltage of the lock-in amplifier is recorded for 30 s (three times each) and an average value is calculated. The scattered power is obtained by using the calibration factor 345485 W/A m^2 sr for the 38 mm port diameter (see section Calibration). The angle-resolved scattering (ARS) function is derived as a useful approach for evaluation and comparison of the results with theoretical calculations. The ARS function is defined as follows:[17]

$$ARS(\theta_s) = \frac{dP_s(\theta_s)}{d\Omega P_i} \tag{1}$$

where θ_s denotes the scattering angle relative to the surface normal. P_s and P_i are the scattered and the incident power and $d\Omega$ is the solid angle of the detection system. The ARS function is equivalent to the cosine-corrected bidirectional scattering distribution function (BSDF):[16] ARS(θ_s)= cos θ_s· BSDF. In this study, the detection area and the solid angle of the scattered radiation from the surface are $3.84 \cdot 10^{-5} m^2$ and $9.62 \cdot 10^{-4} sr$, respectively. The samples and the results of the light scattering measurements are described in more detail in the following sections.

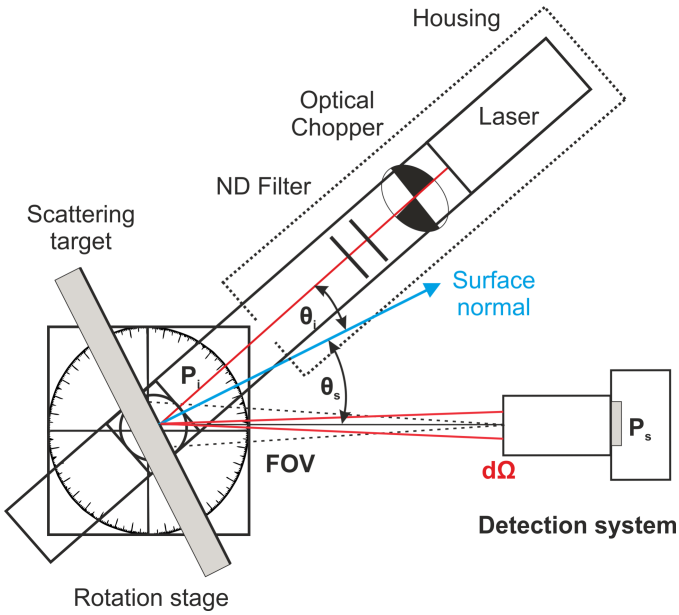

Figure 8: Sketch of the experimental setup for the light scattering measurements.

4.2 Material

A polytetrafluoroethylene (PTFE)-based sample (OptoPolymer, Berghof Fluoroplastic Technology) served as well-established reference material for diffuse reflection measurements. Furthermore, two custom-built aluminum samples with different surface roughnesses are investigated (see Figure 9). Selected physical and optical properties of the samples are summarized in Table 2. The samples are characterized using a white light interferometry (WLI) microscope (Wyko NT9100, Veeco) with a 2.5x objective. For this purpose, WLI images are recorded at four positions on the samples with a size of 2.53 x 1.90 mm. Figure 10 shows exemplary WLI images of the examined samples with the corresponding roughness values (i.e arithmetic average roughness (Ra) and root-mean-squared (RMS) roughness (Rq)). It can be seen that the PTFE-based sample has the highest roughness values of the examined samples, which is probably related to its porous structure.[18] The values for the highest peak and lowest valley are 13 μm and -5 μm, respectively. The WLI image of the rolled aluminum sample shows marked grooves due to the manufacturing process. The average Ra/Rq values are 0.668 μm and 1.034 μm, respectively. The traces of the polishing tool are visible in the WLI image of the polished aluminum sample resulting in average Ra/Rq values of 0.115 μm and 0.169 μm, respectively. In the case of the polished aluminum sample, specular reflections of surrounding objects can be visually observed.

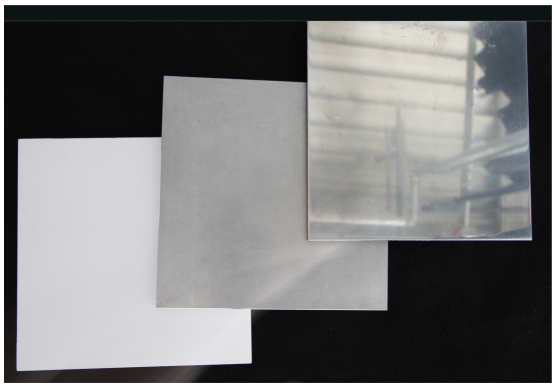

Figure 9: Photograph of the investigated samples. Please see Table 2 for details.

Table 2: Samples used for the light scattering measurements

	#1	#2	#3
Manufacturer	Berghof Fluoroplastic Technology	Schneider Präzisionstechnik	Schneider Präzisionstechnik
Material	Optical PTFE	Aluminum	Aluminum
Density [g/cm^3]	1.5	2.69	2.69
Average Ra [μm]	1.286	0.668	0.115
Average Rq [μm]	1.683	1.034	0.169
Reflectance at 1030 nm	98.18%[a]	94.36%[b]	94.36%[b]

[a] The reflectance value is provided by a figure of the manufacturer.[19]
[b] The values are room-temperature normal-incidence reflectances of bare aluminum, which are taken from the literature.[20]

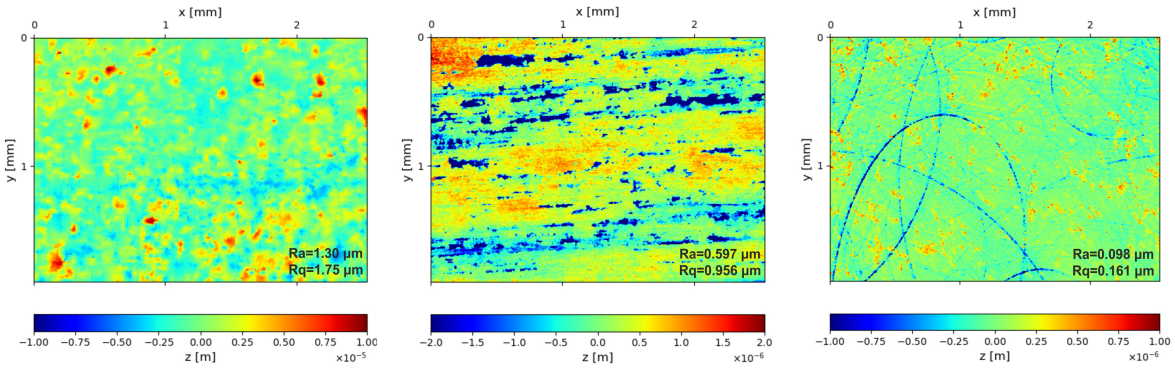

Figure 10: Pseudo-color coded white-light interferometry (WLI) images of the investigated samples. Please note the different scaling of the z axes.

4.3 Light scattering experiments

For the evaluation of the light scattering measurements of the PTFE-sample (OptoPolymer), the maximum voltage signal of each run is normalized to unity and the individual runs are statistically analyzed (see Figure 11). It can be seen from Figure 11 that the results of the two detectors are qualitatively in agreement with the expected $cos\,\theta_s$ behavior, which is characteristic for an ideal diffuse reflector.[18] At a closer look, the results are in line with findings for Spectralon® at an incident angle of 30°, a wavelength of 700 nm, and p-polarized scattering measurements.[21] Parretta et al. reported similar findings for Spectralon® at incident angles of 10° and 40° for incident unpolarized radiation at 1064 nm.[18] It should be noted that the variation of the experimental data is greater for the PDA compared to the PMT. This result may be related to the slightly outstanding first run of the measurements with the PDA. At large scattering angles (i.e. $> 80°$) a leveling off is observed indicating that the lower limit of detection at the selected gain settings is reached.

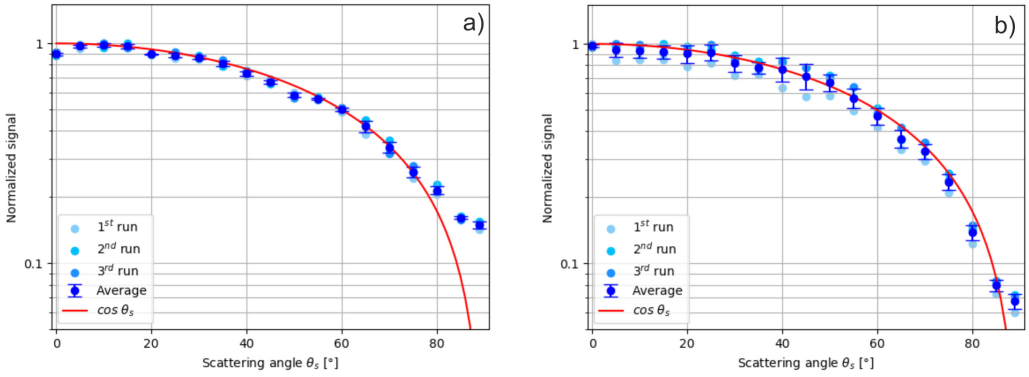

Figure 11: Normalized signal as a function of the scattering angle for the PTFE-based sample (OptoPolymer). The light scattering measurements are performed with a) PMT and b) PDA. The laser wavelength and the angle of incidence are 1030 nm and 30°, respectively. The error bar corresponds to 1σ.

Figure 12 shows the angle-resolved scattering functions of two aluminum samples measured by the detection system equipped with the PMT. It can be recognized that the ARS functions change with different gain settings of the lock-in amplifier. At low amplification, the directed component can be captured well. However, scattering at smaller and larger angles than the specular direction is drowned out by the noise of the detection system. Increasing the amplification enables the detection of scattered laser radiation at smaller or larger scattering angles with the restriction that the lock-in amplifier may become saturated in the region of the directed component (see Figure 12b). To resolve the complete ARS function of an aluminum sample, several runs at different gain settings should be acquired. It should be kept in mind that increasing the gain also increases the noise level.

The results are compared to the microroughness model of pySCATMECH, which is based on the Rayleigh-Rice theory for the scattering of smooth surfaces.[22] The following ABC parameters of the power spectral density (PSD) are used to fit the light scattering measurements with the PMT: A=0.1, B=110, and C=1.25 for aluminum sample #2 and A=0.35, B=280, and C=1.8 for aluminum sample #3. For the measurements with the PDA the parameters are: A=0.025, B=110, and C=1.5 for aluminum sample #2 and A=0.1, B=280, and C=1.65 for aluminum sample #3. The incident polarization and the polarization sensitivity of the detector are set to the stokes vector [1,1,0,0] corresponding to horizontally linearly polarized radiation. Both aluminum samples can not be considered optically smooth in terms of the Rayleigh criterion so that the validity of the model fits is limited. Figure 13 shows the ARS functions of two aluminum samples measured by the detection system equipped with the PDA. In contrast to the light scattering measurements with the PMT, no variations in the gain settings of the transimpedance amplifier have been studied. From the Figures 12 and 13 it can be concluded that both detectors give comparable results and are capable of measuring the ARS function of solid point light sources in a controlled environment.

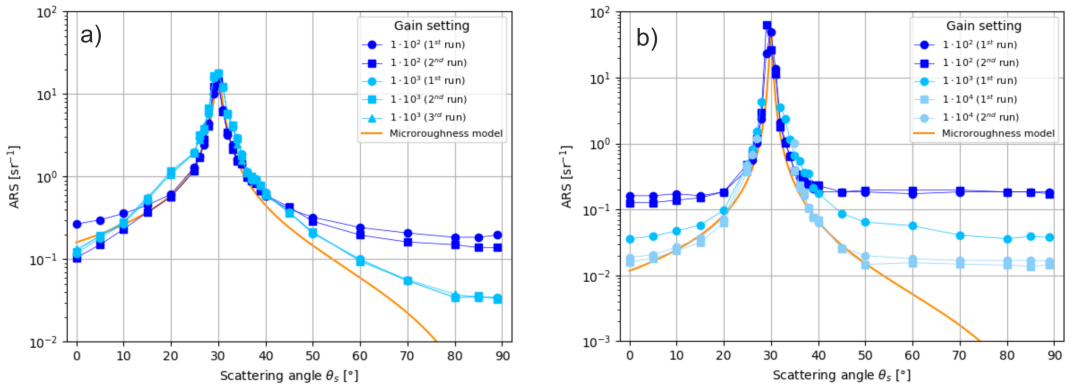

Figure 12: Angle-resolved scattering functions of two machined aluminum samples measured with the PMT at selected gain settings of the lock-in amplifier. a) and b) correspond to different surface roughnesses of the samples (see Table 2 for details.)

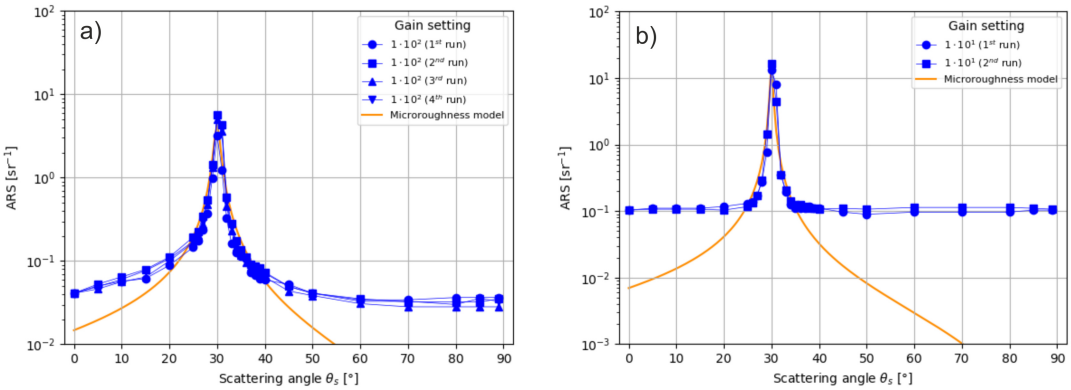

Figure 13: Angle-resolved scattering functions of two machined aluminum samples measured with the PDA at selected gain settings of the transimpedance amplifier. The gain of the lock-in amplifier is set to 10^4. a) and b) correspond to different surface roughnesses of the samples (see Table 2 for details.)

4.4 Peripheral devices

The functioning of the peripheral sensors has been checked by performing measurements over several days on the DLR laser test range in Lampoldshausen. For example, the detection system is placed in the middle of the laser test range and the position is determined with either a single GPS module (without RTK mode) or with both GPS modules (i.e. rover and base station operation in RTK mode). An accuracy of ± 2.5 m without RTK mode and ±7 cm with RTK fixed mode is found (see Figure 14). However, it should be noted that environmental conditions or signal blockage by buildings can significantly reduce the positioning accuracy of the system. By comparing the weather sensor and the PM sensor with certified permanently installed sensors on the laser test range, a reasonable correlation of the data is observed. Last but not least, the video camera can be used to generate high-quality images and videos at short distances with the wide-angle lens and large distances up to 130 m with the zoom lens. Field tests of the peripheral sensors are an important step for the future deployment of the detection system as they can provide additional information about the environment compared to the light scattering measurements.

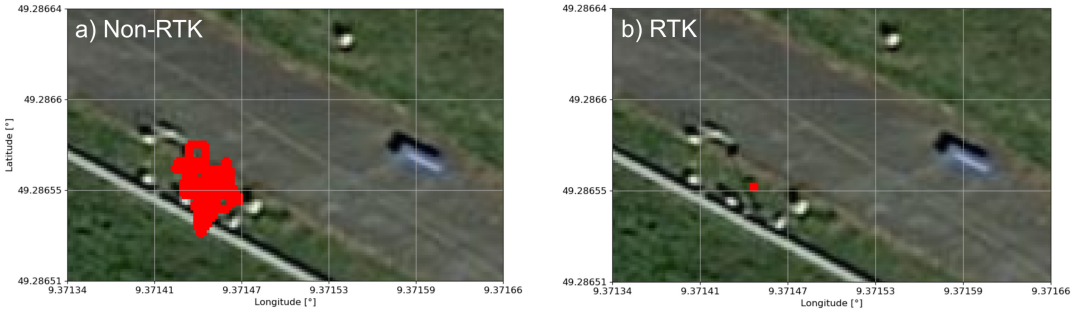

Figure 14: Geographic map of the DLR laser test range superimposed by the GPS coordinates of the detection system in a) non-RTK mode and b) RTK fixed mode.

5. CONCLUSIONS AND OUTLOOK

A wavelength-specific radiometric detection system has been developed for measuring the scattered laser radiation in outdoor environments. A two-step calibration procedure allows converting the measured voltage into absolute scattered powers. The detection system is characterized by using light scattering measurements of solid samples (i.e. a PTFE-based and two aluminum samples) in a laser safety enclosure. The samples are selected according to their scattering properties ranging from ideal diffuse reflection to a mixture of diffuse and specular reflection. It could be shown that the detection system equipped with different detectors delivers reproducible results. The light scattering measurements are in reasonable agreement with theoretical calculations and numerical models.

Light scattering experiments on the DLR laser test range in Lampoldshausen are planned for the near future. For this purpose, the detection system will be placed at different positions in relation to the laser beam and target, and the scattered laser radiation from an irradiated target or atmospheric particles is monitored. A spatially resolved hazard map of the scattered laser radiation can be generated based on the measurements. Furthermore, the software-based data acquisition and processing will be improved. A graphical user interface (GUI) will be developed, where the relevant parameters for the operator are displayed in a processed format. It is intended to repeat the calibration procedure of the detection system at a higher modulation frequency of the laser (i.e 100 or 200 Hz). This could reduce the contribution of the noise and leads to higher accuracy of the measured scattered power.

ACKNOWLEDGMENTS

The authors would like to thank Björn Prietzel, Thomas Schlagenhaufer, and Ralf Zimmermann for their technical support and Kirsten Klaffki for the preparation of CAD drawings of the environmental housing of the detection system. Gabriele Taube is thanked for performing the white-light interferometry measurements. Daniel Schwefel is acknowledged for providing the spectroradiometer data of the first calibration step.

REFERENCES

1. Böker, D., Schwarz-Hemmert, C., and Netzler, D., "Quantitative laser safety analysis for application of high-energy lasers in a field test," in [*Laser Technology for Defense and Security X*], Dubinskii, M. and Post, S. G., eds., **9081**, 49 – 63, International Society for Optics and Photonics, SPIE (2014).
2. American National Standards Institute, [*ANSI Z136.6 - Safe use of lasers outdoors*], Laser Institute of America, Orlando, FL 32826 (2015).
3. Royston, D. D., "An accurate laser radiometer for determining visible exposure times," *Lasers in Surgery and Medicine* **5**(5), 519–527 (1985).
4. Corder, D., Evans, D., and Tyrer, J., "An intelligent maximum permissible exposure meter for safety assessments of laser radiation," *Optic and Laser Technology* **28**(6), 409 – 415 (1996).
5. Corder, D., Evans, D., and Tyrer, J., "An improved maximum permissible exposure meter for safety assessments of laser radiation," *Optics and Lasers in Engineering* **28**(6), 423 – 442 (1997).
6. Corder, D., Evans, D., Tyrer, J., Freeland, C., and Myler, J., "High power laser beam delivery monitoring for laser safety," *Optics and Lasers in Engineering* **27**(5), 479 – 492 (1997).
7. Gigahertz Optik GmbH, "BTS2048-VL-TEC with LDM-1901." https://www.gigahertz-optik.com/en-us/product/bts2048-vl-tec-with-ldm1901/ (2021).
8. Sliney, D. H., "Radiometry and laser safety standards," *Health Physics* **56**(5), 717–724 (1989).
9. Daigle, J.-F., Pudo, D., Théberge, F., and Châteauneuf, M., "Laser safety evaluation for high-energy laser interaction with solids," *Optical Engineering* **56**(2), 1 – 7 (2017).
10. Henrichsen, M., Schwarz, B., Ritt, G., Azarian, A., and Eberle, B., "Laser safety assessments supported by analyses of reflections frommetallic targets irradiated by high-power laser light," *Appl. Opt.* **60**, F71–F87 (Aug 2021).
11. American National Standards Institute, [*ANSI Z136.1 - Safe Use of Lasers*], Laser Institute of America, Orlando, FL 32826 (2000).
12. European Union, "Directive 2006/25/EC of the European Parliament and of the Council of 5 April 2006 on the minimum health and safety requirements regarding the exposure of workers to risks arising from physical agents (artificial optical radiation) (19th individual Directive within the meaning of Article 16(1) of Directive 89/391/EEC)," (2019).
13. Mishchenko, M. I., "Measurement of electromagnetic energy flow through a sparse particulate medium: A perspective," *Journal of Quantitative Spectroscopy and Radiative Transfer* **123**, 122 – 134 (2013). Peter C. Waterman and his scientific legacy.
14. Mishchenko, M. I., "Directional radiometry and radiative transfer: The convoluted path from centuries-old phenomenology to physical optics," *Journal of Quantitative Spectroscopy and Radiative Transfer* **146**, 4 – 33 (2014). Electromagnetic and Light Scattering by Nonspherical Particles XIV.
15. Pargmann, C., Becker, P., Peckhaus, A., and Duschek, F., "Angle dependent stray light measurements of high-power laser radiation in natural atmospheric environments," 15 (10 2018).
16. Stover, J. C., [*Optical scattering : measurement and analysis*], SPIE Optical Engineering Press Bellingham, Wash., USA, 2nd ed. ed. (1995).
17. Schröder, S., Duparré, A., Coriand, L., Tünnermann, A., Penalver, D. H., and Harvey, J. E., "Modeling of light scattering in different regimes of surface roughness," *Opt. Express* **19**, 9820–9835 (May 2011).
18. Parretta, A. and Addonizio, M., "Optical and structural characterization of diffuse reflectance standards," *International Journal of Optics and Applications* **5**, 33–49 (05 2015).
19. Berghof Fluoroplastic Technology GmbH, "Reflection standards." https://optopolymer.de/wp-content/uploads/2018/05/OptoPolymer-en.pdf (2018).
20. Bass, M., Stryland, E. W. V., Williams, D. R., and Wolfe, W. L., [*Handbook of optics - Devices, Measurements, and Properties*], vol. II, New York, NY: McGraw-Hill, 2nd ed. (1995).
21. Lévesque, M. P. and Dissanska, M., "Measurement and modeling of the Spectralon™ spectro-polarimetric bidirectional reflectance distribution function (BRDF)," Tech. Rep. DRDC-RDDC-2016-R221, DRDC – Valcartier Research Centre (2016).
22. Germer, T. A., "pySCATMECH: a Python interface to the SCATMECH library of scattering codes," in [*Reflection, Scattering, and Diffraction from Surfaces VII*], Hanssen, L. M., ed., **11485**, 43 – 54, International Society for Optics and Photonics, SPIE (2020).